Manuscript ID: DOEBTO-UMD-9681-25-AO

Full citation: Othman, A., Aute, V., and Tancabel, J. "**Influence of Phase-Change Materials and Operating Periods on Load Shifting for Thermal Storage Heat Pumps in European Climate Zones.**" *Proceedings of the 15th REHVA HVAC World Congress - CLIMA 2025*. Politecnico di Milano – Campus Bovisa, Milan, Italy

Influence of Phase-Change Materials and Operating Periods on Load Shifting for Thermal Storage Heat Pumps in European Climate Zones

Al-Hussain Othman[1], Vikrant Aute[1*], James Tancabel[1]

[1] Center for Environmental Energy Engineering
Department of Mechanical Engineering, University of Maryland
College Park, MD 20740, USA
[*]Corresponding author's email: vikrant@umd.edu

Abstract. As the reliance on heat pumps (HPs) for space conditioning increases worldwide, extensive grid strains during utility peak hours are expected. Significant research efforts focus on investigating the use of integrated thermal energy storage (TES) systems to reduce peak energy demands. Conventionally, TES systems are often integrated to store and provide either cooling or heating, but not both. In this work, a single room-temperature phase-change material (PCM)-TES was integrated for dual-mode operation with an R290 air-to-water 10.5 kW (3-Ton) HP. Two PCM melting temperatures (17°C, 22°C) were assessed to investigate their impact on system performance and cost reductions for Milan, Italy (4A); Barcelona, Spain (3A); and Oslo, Norway (6A). HP and HP-TES performance maps were generated using Modelica-based transient models and co-simulated with a prototype residential building using the Spawn of EnergyPlus™ with simple rule-based controls. Our simulations indicate that PCM-17°C provided annual cost savings at higher peak-to-off-peak cost ratios, as the demand reduction dominated the savings potential. The recharge energy costs and requirements became more dominant at lower cost ratios, making PCM-22°C more beneficial at lower cost ratios. Finally, despite Oslo's heating-dominated climate, the utility peak hours favor cooling demand reductions, making PCM-17°C more appealing. In all cases, the cost savings potential stabilized between 4 – 10% regardless of cost ratio, suggesting that system-level component and operation control optimization is required to maximize cost savings further.

Keywords: Thermal energy storage, Phase-change material, HP-TES performance maps, Cost savings.

1 INTRODUCTION

As the number of heat pumps (HPs) grows with continuous decarbonization efforts [1], power grid strains become inevitable to meet the required building loads. The addition of intermittent renewable energy sources can introduce grid instabilities, further increasing peak demands and raising the need for energy storage systems [2]. Thermal energy storage systems have significant potential in systems that require or use thermal energy, especially space cooling and heating systems [3].

Integrated heat pump thermal energy storage (HP-TES) and its control procedures have significant research efforts. Drees & Braun [4] investigated the potential of a chiller-ice thermal storage by comparing rule-based and optimal control strategies. An integrated HP-TES system can achieve cost savings due to demand reductions using robust and optimal controllers, such as model predictive controllers (MPCs), given their flexibility in handling dynamic peak hours[5 - 6]. However, MPCs are often much more complex to develop and operate than rule-based controllers (RBCs), as they focus on load shifting while disregarding hourly optimizations [7]. Thus, we utilized RBCs to identify the most suitable PCM temperature(s) for the HP-TES for a given region. Additionally, we see that the development of optimal controls should come after first improving HP-TES components.

In this work, an R290-based 10.5 kW (3-ton) HP-TES unit was designed and simulated for use in three European cities: (i) Milan, Italy, (ii) Barcelona, Spain, and (iii) Oslo, Norway, using two different PCM melting temperatures (17°C, 22°C) to determine the impact of PCM melting temperature on overall system performance and potential cost savings. Co-simulations using the Spawn of EnergyPlus™ [8] were conducted for the prototype single-family residence [9 -10] using IWEC-TMY weather data [11]. An RBC strategy was developed assuming static daily peak-hour periods. Recommendations for the TES PCM melting temperatures were provided depending on the location and associated cost savings.

2 METHODOLOGY

2.1 System Cycle and Component Modeling

The R290 dual-purpose air-to-water HP-TES shown in Fig. 1 was sized for a 10.5 kW (3-ton) cooling and heating capacity at AHRI 210/240 A and H1 conditions. These conditions correspond to outdoor dry-bulb and wet-bulb temperatures of 35°C and 23.8°C for the A-Test, and 8.3°C and 6.1°C for the H1-Test [12]. The operating modes, described in detail in Othman et al. [13] (Fig. 1), reduce peak electrical demand for space conditioning by lowering the temperature lifts of the system, thereby decreasing the compressor power.

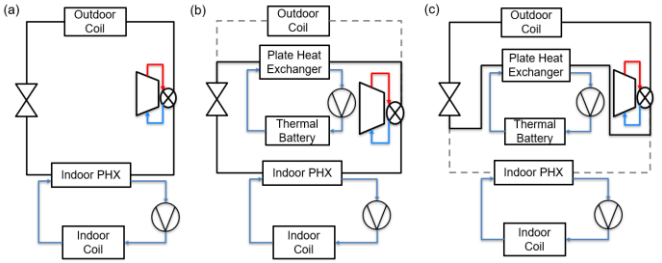

Fig. 1. HP-TES system:
(a) Baseline HP unit; (b) HP-TES unit discharge mode; (c) HP-TES unit recharge mode

The thermal battery was sized to operate for 2 continuous hours for two PCMs with distinct melting temperatures of 17°C and 22°C and similar thermodynamic properties [14]. The 2-hour operating period was selected since HP-TES systems have shown high demand reductions during the most extreme (i.e., highest/lowest) ambient temperature hours, which oftentimes coincide with utility peak hours [3 - 13]. Furthermore, longer TES operating periods will yield larger TES systems with extensive PCM requirements, which may be infeasible in existing building structures. The storage capacity was determined using Eq. (1), where the maximum required discharge rate $\dot{Q}_{dis}$ is for cooling mode, i.e., accounting for both the cooling capacity and compressor power at AHRI 210/240 A-Test operating conditions. Using multiple finned-tube heat exchangers with an outer tube diameter of 9.5 mm, the surface areas were computed based on the maximum required using the UA-LMTD approach, as done in [13]. Furthermore, the fin density was selected to ensure the appropriate PCM volume availability and UA requirements.

$$V_{PCM,req} = \frac{\int_{t=0}^{t=2hr} \dot{Q}_{dis} dt}{\rho_{PCM} \cdot H_{sl}} \tag{1}$$

The HP-TES was modeled using an in-house Modelica Library [15]. The indoor air-water heat exchanger was a tube-fin HX with 3 control volumes (CVs): water, wall, and air, where axial conduction was neglected. The water CV is segmented to account for different heat transfer coefficients and pressure drops along the HX using the Dittus-Boelter and Churchill correlations, respectively [16 - 17]. The air CV considers both sensible and latent loads, taking into account fin efficiencies and correcting the Wang et al. [18] airside heat transfer coefficient using the Lewis analogy [19].

The outdoor air-to-refrigerant HX uses the same CV strategy, only replacing the water CV with a refrigerant CV. The Shah [20 - 21] correlations were used for the two-phase heat transfer coefficients for boiling and condensing flows, respectively. Similarly, the two-phase pressure drops were determined using Xu-Feng (boiling) and Cavallini et al. (condensing) correlations [22 - 23]. The Dittus-Boelter and Churchill correlations [16 - 17] were used in all single-phase regions. In all HXs, the wall CV solves the transient energy balances from the two fluids, accounting for the thermal capacity of the tube walls and fins. In this study, the defrost cycles were not considered.

The TES (PCM-HX) and indoor air-water HXs are connected to the HP using hydronic secondary loops consisting of a brazed plate HX and a pump (Fig. 1b,c). A commercial selection tool was used to size the plate HX, where the model details can be found in [13]. The single-speed compressor, selected from Alabdulkarem et al. [24], was modeled using the manufacturer-provided 10-coefficient compressor map as per AHRI Standard 540 [25]. The EXV was modeled with a PI controller, adjusting the opening based on the required suction superheat.

The TES was modeled using the capacitance-resistance approach. The capacitance represents the enthalpy of fusion in the two-phase melting region (Eq. (2)) obtained from the PCM manufacturer DSC curves [14]. The resistance in Eq. (3) shows the PCM heat transfer coefficients during the phase-change process. The characteristic length L is the half-distance between two HX tubes. The TES assumed adiabatic conditions on all external boundaries.

$$\dot{Q}_{PCM} = \frac{di}{dt} M_{PCM} \tag{2}$$

$$\dot{Q}_{PCM} = \frac{k_{PCM}}{L} \sum_{j=1}^{j=N_{seg}} A_{seg,j} (T_{wall,j} - T_{water,j-1}) \tag{3}$$

2.2 HP-TES System Performance Mapping

System-level performance maps were developed for the baseline HP and HP-TES in cooling and heating modes based on ASHRAE Standard 205 [26 - 27]. Annual simulations using the DOE prototype single-family residential building were conducted with the Spawn of EnergyPlus™ [8 - 10]. The system map for the baseline HP system in cooling mode (Eq. (4)) is a bi-quadratic function of the indoor wet-bulb and outdoor dry-bulb temperatures. The fan and pump powers were considered according to the HP-TES operating mode. The maps were developed for an outdoor dry-bulb temperature range of 18 – 45°C and an indoor coil relative humidity range of 25 – 90%. Similar to the cooling mode, heating mode maps were developed (Eq. (5)), however, auxiliary heating (with COP = 1) was considered when the off-coil heat pump supply temperature was below 32°C, per ASHRAE Standard 90.1 [28]. The heating performance map's operating range for outdoor dry-bulb temperature was -15 – 13°C, while the indoor dry-bulb temperature range was 10 – 25°C. When the outdoor temperatures were below -15°C, heating was provided solely by the backup heating system.

$$\begin{bmatrix} \dot{Q}_{cap} \\ COP \end{bmatrix} = \begin{bmatrix} [C_1 ... C_6]_{\dot{Q}} \\ [C_1 ... C_6]_{COP} \end{bmatrix} f(T_{wb,in}, T_{db,out}) \tag{4}$$

$$\begin{bmatrix} \dot{Q}_{cap} \\ \dot{W}_{sys} \end{bmatrix} = \begin{bmatrix} [C_1 ... C_6]_{Q} \\ [C_1 ... C_6]_{\dot{W}} \end{bmatrix} f(T_{db,in}, T_{db,out}) \qquad COP_{heat} = \frac{\dot{Q}_{cap,heating} + \dot{Q}_{aux}}{\dot{W}_{sys} + \dot{Q}_{aux}} \tag{5}$$

In the HP-TES modes, the TES outlet water temperature was used as an input to the HP-TES maps (Eq. (6)) for both discharge and recharge operations. This water temperature also served as an indicator of the TES state of charge (SOC), i.e., the relative ratio of utilized TES storage to the full TES storage potential. To this end, the discharge and recharge processes were initiated/terminated based on the instantaneous TES outlet water temperature.

The initial and final PCM temperatures were set for all modes based on DSC curves from the PCM manufacturer [14]. The water temperature is a function of time and outdoor/indoor dry-bulb temperatures, depending on the operating mode, i.e., recharge mode (outdoor) or discharge mode (indoor), as shown in (Eq. (6)).

Discharge operation:	Recharge operation:
$T_{w,out} = f(T_{wb,in} \text{ or } T_{db,in}, t)$	$T_{w,out} = f(T_{db,out}, t)$
$\dot{Q}_{cap} = f(T_{wb,in} \text{ or } T_{db,in}, T_{w,out})$	$\dot{Q}_{cap} = 0$
$\dot{W}_{total} = f(T_{wb,in} \text{ or } T_{db,in}, T_{w,out})$	$\dot{W}_{total} = f(T_{db,out}, T_{w,out})$
$\dot{Q}_{PCM} = f(T_{wb,in} \text{ or } T_{db,in}, T_{w,out})$	$\dot{Q}_{PCM} = f(T_{db,out}, T_{w,out})$

(6)

The rule-based control algorithm was developed such that HP-TES discharge occurs during the utility peak periods until the PCM storage is fully exhausted, i.e., zero SOC. As this work focused on reducing peak energy demands and shifting them to off-peak hours, the TES was recharged at the most suitable off-peak nocturnal hours when space conditioning was not required. During all other hours, the baseline HP provides space conditioning. The indoor thermostat temperature sets the building demand: in cooling mode, the indoor temperature cooling setpoints were 24°C ± 1 K while heating indoor setpoints were 21°C ± 1 K. Three European cities (Table 1), Barcelona (warm), Milan (moderate), and Oslo (cold) were chosen to investigate the impact of different PCM melting temperatures across multiple European climate zones. The corresponding peak utility hours for each location are also listed in Table 1.

Table 1. Peak hours and climate zones for the 3 selected cities

Location	Climate Zone	Peak Hours
Barcelona, Spain	Warm, Humid (3A)	10 AM – 2 PM & 6 PM – 10 PM [29]
Milan, Italy	Mixed, Humid (4A)	8 AM – 7 PM [30]
Oslo, Norway	Cold, Humid (6A)	4 PM – 10 PM [31]

Finally, the operating cost savings were determined using Eq. (7). The first term represents the peak demand reduction, while the second term is the cost increase associated with off-peak recharging of the TES. The peak-to-off-peak cost ratio was iterated to find the minimum required ratio to yield annual operating cost savings for the HP-TES system.

$$\%c_{savings} = \left(\frac{E_{HP,peak} - E_{dis,TES}}{E_{HP,peak}} - \frac{c_{off,peak}}{c_{peak}} \frac{E_{rech,TES}}{E_{HP,peak}} \right) \times 100 \quad (7)$$

3 RESULTS AND DISCUSSION

Fig. 2a,b presents the improvements in system COP for the HP-TES for cooling and heating, respectively. The HP-TES COP improvement occurs over a range that is bounded between the horizontal lines (Fig. 2a,b), corresponding to the PCM solidus and liquidus temperatures. As expected, the highest COP improvements are at the hottest (cooling mode) or

coldest (heating mode) temperatures, respectively, as these correspond to the largest reductions in temperature lift. Additionally, this explains why the PCM-17°C has a higher COP improvement in cooling mode, whereas PCM-22°C has a slightly higher COP improvement in heating mode (Fig. 2b).

Simulation results for a full summer day in Milan (July 4) are shown in Fig. 3. It can be seen that PCM-17°C achieves higher demand reductions and operates longer during peak hours (after 8 AM), mainly due to higher delivered to the indoor space. However, the TES system based on PCM-17°C has a longer and more energy-intensive recharge process compared to PCM-22°C due to the higher system temperature lift.

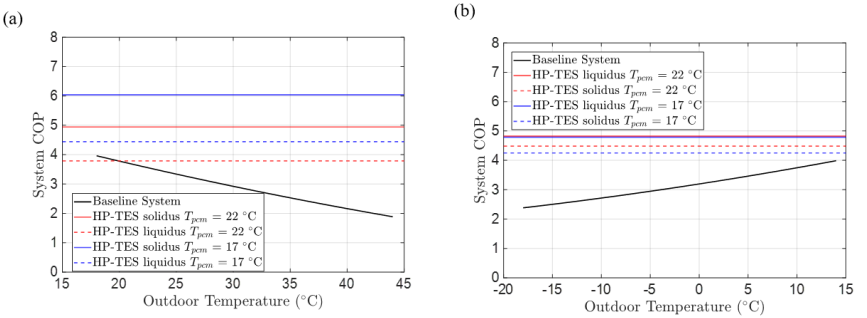

Fig. 2. HP-TES vs. Baseline COP for two PCMs (17°C, 22°C): (a) Cooling; (b) Heating

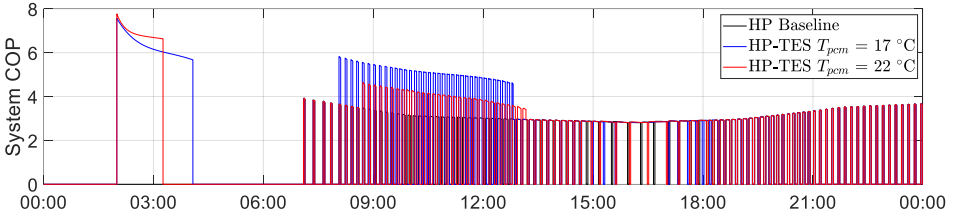

Fig. 3. Overall system COP for a cooling day (July 4) in Milan, Italy

The system-level maps were simulated for all 3 locations; IWEC-TMY [11] weather data shows the summer average outdoor temperature ranges in Barcelona and Milan are between 26 – 29°C, resulting in a higher overall cooling mode demand reduction for PCM-17°C compared to PCM-22°C (Fig. 4a). On the other hand, using a PCM with lower melting temperature in cooling mode has two penalties: (i) increased recharge energy requirements during summer months (higher recharge temperature lifts) and (ii) reduced peak demand reduction during winter months (higher peak hour temperature lifts).

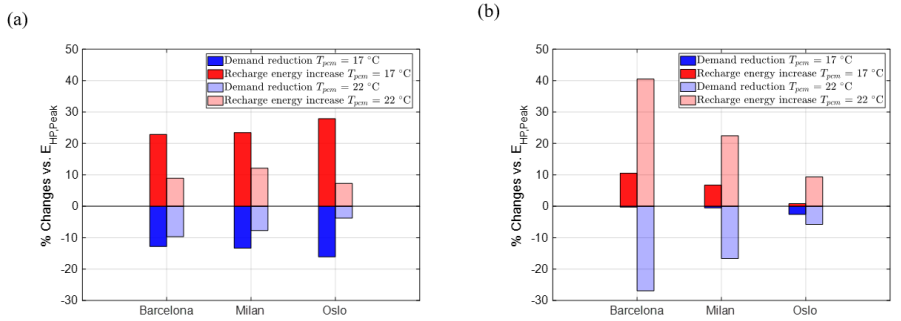

Fig. 4. Demand reductions and recharge energy increases compared with peak energy requirements for (a) summer months and (b) winter months

The simulation results for Oslo, however, are more interesting. Although Oslo has a heating-dominated cold climate (Table 1), the heating mode demand reductions were lower than cooling for two main reasons. First, the utility peak hours are 4 – 10 PM year-round, favoring cooling demand reductions as they coincide with higher outdoor temperature hours; on the other hand, heating demand peaks during utility off-peak hours in the early morning / late night. The second reason relates to the PCM melting temperatures considered herein; it may be possible that even higher temperature PCMs would be favored for such a climate to reduce peak heating demands further. This was observed in Fig. 3b, as PCM-22°C outperforms PCM-17°C during winter. To understand the overall annual demand reduction (i.e., more dominant in cooling/heating), the annual aggregate demand reductions and recharge energies were assessed (Fig. 5a). Furthermore, the annual cost savings were determined for peak cost ratios from 1 to 10, as shown in Fig. 5b.

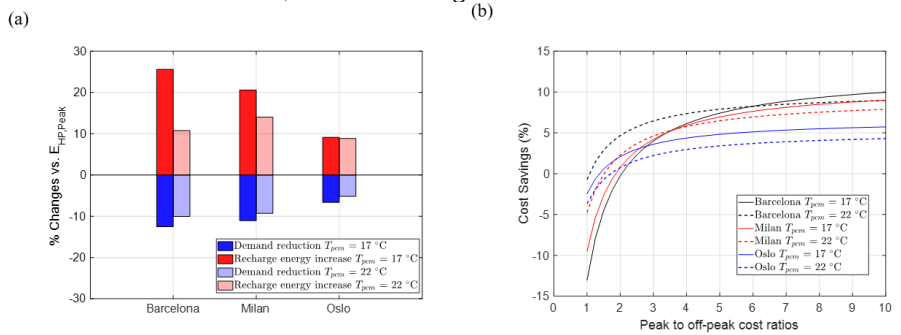

Fig. 5. (a) Aggregate annual demand reductions and recharge energy increases, (b) Annual operating cost savings for different peak energy cost ratios

Comparing the aggregates (Fig. 5a), no net reductions in annual energy consumption were found for the proposed HP-TES system, given the gap between peak demand reduction and recharge energy increase. To limit this gap, several paths can be considered, including but not limited to adopting optimal control strategies, optimization of the TES HXs, and

using variable-speed equipment, i.e., compressors and pumps. However, the PCM melting temperature was found to be a crucial aspect of minimizing this gap. This suggests that selecting the TES melting temperature is a location-specific consideration.

On the other hand, cost savings were found to be possible but largely dependent on the peak energy cost ratio (Fig. 5b). For all considered cities and PCMs, a near-constant cost savings percentage was achieved for higher cost ratios (> 4). This occurs since the cost savings become dominated by the peak demand reduction (Eq. (7)). Thus, from Fig. 5b, it can be seen that recharge energy mitigation strategies should be a higher priority if the peak-to-off-peak energy cost ratio is 4 or lower. Additionally, for cooling-dominated regions, PCM-17°C provided more savings at higher cost ratios while PCM-22°C had higher cost savings at lower ratios; this is due to the lower recharge energy requirement. In Oslo, the peak hours and lower temperature PCMs favored cooling mode, and the lower temperature PCM was favored at all cost ratios, again due to the lower recharge energy.

4 CONCLUSIONS

In this work, a dual-purpose air-to-water R-290 10.5 kW (3-Ton) HP-TES system was simulated in Modelica for 3 European cities (Barcelona, Milan, Oslo) for two PCMs with melting temperatures of 17°C and 22°C. Operational cost savings potential was assessed by comparing HP and HP-TES operations. It was found that at higher peak-to-off-peak cost ratios (> 6), PCM-17°C can result in higher cost savings (10%) in cooling-dominated regions due to peak demand savings resulting from reduced temperature lifts becoming the dominant cost factor. On the other hand, recharge energy costs play a larger role for lower cost ratios (< 2.5), and thus PCM-22°C can be more beneficial with cost savings between 1 – 4%. In Oslo, a heating-dominated climate, the year-round constant utility peak hours favored cooling mode operation and thus resulted in more significant cooling mode savings. Given that the present HP-TES system was intended to operate solely during the utility peak hours, many opportunities arise to achieve greater energy and cost savings by considering component improvements, location-specific PCM melting temperatures, and adopting optimal control strategies.

NOMENCLATURE

C	Map coefficients [-]
C	Utility cost, \$ kWh^{-1}
E	Energy kWh
H_{sl}	Enthalpy of Fusion kJ kg^{-1}
k	Thermal conductivity, W m^{-1} K^{-1}
Q	Heat transfer, kW
T	Temperature, °C
W	Electrical power, kW
Greek symbols	
ρ	Density, kg m^{-3}

Acronyms

IWEC	International Weather for Energy Calculations
TMY	Typical Meteorological Year

REFERENCES

[1] IEA, “Is cooling the future of heating? – Analysis,” IEA. Accessed: Feb. 13, 2024. [Online]. Available: https://www.iea.org/commentaries/is-cooling-the-future-of-heating

[2] F. Cebulla, J. Haas, J. Eichman, W. Nowak, and P. Mancarella, “How much electrical energy storage do we need? A synthesis for the U.S., Europe, and Germany,” *J. Clean. Prod.*, vol. 181, pp. 449–459, Apr. 2018, doi: 10.1016/j.jclepro.2018.01.144.

[3] J. Hirschey, Z. Li, K. R. Gluesenkamp, T. J. LaClair, and S. Graham, “Demand reduction and energy saving potential of thermal energy storage integrated heat pumps,” *Int. J. Refrig.*, vol. 148, pp. 179–192, Apr. 2023, doi: 10.1016/j.ijrefrig.2023.01.026.

[4] K. H. Drees and J. E. Braun, “Development and Evaluation of a Rule-Based Control Strategy for Ice Storage Systems,” *HVACR Res.*, vol. 2, no. 4, pp. 312–334, Oct. 1996, doi: 10.1080/10789669.1996.10391352.

[5] F. D’Ettorre, P. Conti, E. Schito, and D. Testi, “Model predictive control of a hybrid heat pump system and impact of the prediction horizon on cost-saving potential and optimal storage capacity,” *Appl. Therm. Eng.*, vol. 148, pp. 524–535, Feb. 2019, doi: 10.1016/j.applthermaleng.2018.11.063.

[6] D. Fischer, T. R. Toral, K. B. Lindberg, B. Wille-Haussmann, and H. Madani, “Investigation of Thermal Storage Operation Strategies with Heat Pumps in German Multi Family Houses,” *Energy Procedia*, vol. 58, pp. 137–144, Jan. 2014, doi: 10.1016/j.egypro.2014.10.420.

[7] L. Shi, M. Qu, X. Liu, J. Dong, B. Cui, and L. Wang, “Model Predictive Control for a Grid-interactive Efficiency Thermal-storage-integrated Heat Pump System,” *Int. High Perform. Build. Conf.*, Jul. 2022, [Online]. Available: https://docs.lib.purdue.edu/ihpbc/415

[8] Spawn of EnergyPlus, “Spawn-of-EnergyPlus (Spawn),” *Energy.gov*, Accessed: Jul. 27, 2023. [Online]. Available: https://www.energy.gov/eere/buildings/articles/spawn-energyplus-spawn

[9] M. Wetter, “Modelica-based modelling and simulation to support research and development in building energy and control systems,” *J. Build. Perform. Simul.*, vol. 2, no. 2, pp. 143–161, Jun. 2009, doi: 10.1080/19401490902818259.

[10] Dept. of Energy Building Technologies Office, “Prototype Building Models | Building Energy Codes Program,” 2022, Accessed: Nov. 03, 2022. [Online]. Available: https://www.energycodes.gov/prototype-building-models

[11] “ASHRAE International Weather Files for Energy Calculations 2.0 (IWEC2).” Accessed: Dec. 22, 2024. [Online]. Available: https://www.ashrae.org/technical-resources/bookstore/ashrae-international-weather-files-for-energy-calculations-2-0-iwec2

[12] AHRI Standard 210/240, “Standard for Perforamnce Rating of Unitary Air-Conditioing and Air-Source Heat Pump,” 2017.

[13] A. Othman, V. Aute, and J. Tancabel, “Performance Assessment of a Dual-Purpose HP-TES for a Typical Year Comparing Different Climate Zones,” *Int. High Perform. Build. Conf.*, Jan. 2024, [Online]. Available: https://docs.lib.purdue.edu/ihpbc/452

[14] “Solutions,” Insolcorp, LLC. Accessed: Jan. 10, 2025. [Online]. Available: https://insolcorp.com/products/

[15] H. Qiao, V. Aute, and R. Radermacher, “Transient modeling of a flash tank vapor injection heat pump system – Part I: Model development,” *Int. J. Refrig.*, vol. 49, pp. 169–182, Jan. 2015, doi: 10.1016/j.ijrefrig.2014.06.019.

[16] F. W. Dittus and L. M. K. Boelter, “Heat transfer in automobile radiators of the tubular type,” *Univ. Calif. Publ. Eng.*, vol. 12, no. 1, pp. 3–22, Oct. 1930, doi: 10.1016/0735-1933(85)90003-X.

[17] S. W. Churchill, “Friction Factor Equations Spans All Fluid-Flow Regimes,” *Chem. Eng. J.*, vol. 84, pp. 91-92., 1977.

[18] C.-C. Wang, K.-Y. Chi, and C.-J. Chang, “Heat transfer and friction characteristics of plain fin-and-tube heat exchangers, part II: Correlation,” *Int. J. Heat Mass Transf.*, vol. 43, no. 15, pp. 2693–2700, Aug. 2000, doi: 10.1016/S0017-9310(99)00333-6.

[19] K. T. Hong and R. L. Webb, “Calculation of Fin Efficiency for Wet and Dry Fins,” *HVACR Res.*, vol. 2, no. 1, pp. 27–41, Jan. 1996, doi: 10.1080/10789669.1996.10391331.

[20] M. M. Shah, “Unified correlation for heat transfer during boiling in plain mini/micro and conventional channels,” *Int. J. Refrig.*, vol. 74, pp. 606–626, Feb. 2017, doi: 10.1016/j.ijrefrig.2016.11.023.

[21] M. M. Shah, “Improved correlation for heat transfer during condensation in conventional and mini/micro channels,” *Int. J. Refrig.*, vol. 98, pp. 222–237, Feb. 2019, doi: 10.1016/j.ijrefrig.2018.07.037.

[22] Y. Xu and X. Fang, “A new correlation of two-phase frictional pressure drop for condensing flow in pipes,” *Nucl. Eng. Des.*, vol. 263, pp. 87–96, Oct. 2013, doi: 10.1016/j.nucengdes.2013.04.017.

[23] A. Cavallini, D. Del Col, L. Doretti, G. A. Longo, and L. Rossetto, “Heat transfer and pressure drop during condensation of refrigerants inside horizontal enhanced tubes,” *Int. J. Refrig.*, vol. 23, no. 1, pp. 4–25, Jan. 2000, doi: 10.1016/S0140-7007(99)00032-8.

[24] A. Alabdulkarem, R. Eldeeb, Y. Hwang, V. Aute, and R. Radermacher, “Testing, simulation and soft-optimization of R410A low-GWP alternatives in heat pump system,” *Int. J. Refrig.*, vol. 60, pp. 106–117, Dec. 2015, doi: 10.1016/j.ijrefrig.2015.08.001.

[25] AHRI Standard 540, “AHRI 540 (SI/ I-P): Performance Rating of Positive Displacement Refrigerant Compressors and Compressor Units | AHRI,” 2020.

[26] R. T. Muehleisen, C. S. Barnaby, N. Kruis, and T. P. McDowell, “Introduction to ASHRAE 205 – A New Standard for HVAC&R Performance Maps,” 2022.

[27] “ASHRAE Standard 205 Resource Files.” Accessed: Sep. 20, 2024. [Online]. Available: https://data.ashrae.org/standard205/

[28] “Standard 90.1.” Accessed: Jan. 14, 2025. [Online]. Available: https://www.ashrae.org/technical-resources/bookstore/standard-90-1

[29] “Access tariffs,” Endesa. Accessed: Dec. 09, 2024. [Online]. Available: https://www.endesa.com/en/advice/access-tariffs

[30] “Price indexes for electricity and gas.” Accessed: Dec. 09, 2024. [Online]. Available: https://www.cogeserenergia.it/en/price-indexes-for-electricity-and-gas

[31] M. Hofmann and K. B. Lindberg, “Evidence of households’ demand flexibility in response to variable hourly electricity prices – Results from a comprehensive field experiment in Norway,” *Energy Policy*, vol. 184, p. 113821, Jan. 2024, doi: 10.1016/j.enpol.2023.113821.

ACKNOWLEDGMENTS

This material is based upon work supported by the U.S. Department of Energy’s Office of Energy Efficiency and Renewable Energy (EERE) under the Building Technologies Office (BTO) Award Number DE-EE0009681. The views expressed herein do not necessarily represent the views of the U.S. Department of Energy or the United States Government. This work was also supported in part by the Modeling & Optimization Consortium at the Center for Environmental Energy Engineering at the University of Maryland.